IEEE Photonics Journal
An IEEE Photonics Society Publication

Open Access

Fabrication and Characterization of Si Substrate-Free InGaN Light-Emitting Diodes and Their Application in Visible Light Communications

Volume 9, Number 2, April 2017

Chia-Lung Tsai
Ying-Chang Li
Yi-Chen Lu
Sheng-Hsiung Chang

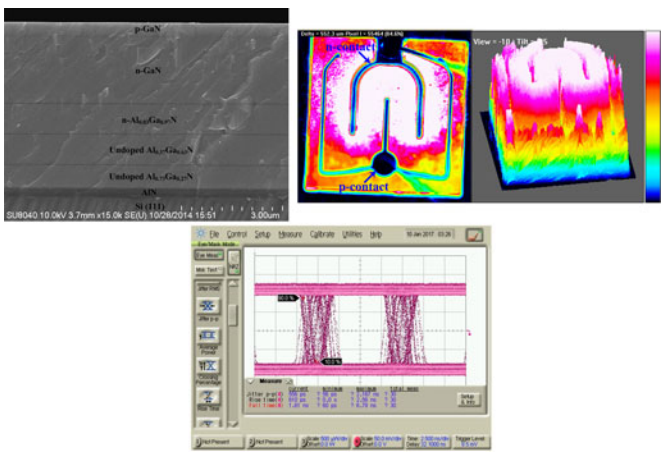

DOI: 10.1109/JPHOT.2017.2683481
1943-0655 © 2017 IEEE

IEEE photonics SOCIETY

IEEE

Fabrication and Characterization of Si Substrate-Free InGaN Light-Emitting Diodes and Their Application in Visible Light Communications

Chia-Lung Tsai,[1] Ying-Chang Li,[2] Yi-Chen Lu,[2] and Sheng-Hsiung Chang[3]

[1]Department of Electronic Engineering and Green Technology Research Center, Chang Gung University, Taoyuan 333, Taiwan, and also with the Department of Otolaryngology-Head and Neck Surgery, Chang Gung Memorial Hospital, Taoyuan 333, Taiwan
[2]Department of Electronic Engineering and Green Technology Research Center, Chang Gung University, Taoyuan 333, Taiwan
[3]Research Center for New Generation Photovoltaics, National Central University, Taoyuan 32001, Taiwan, and also with the Department of Optics and Photonics, National Central University, Taoyuan 32001, Taiwan

DOI:10.1109/JPHOT.2017.2683481

Manuscript received February 16, 2017; revised March 12, 2017; accepted March 13, 2017. Date of publication March 16, 2017; date of current version April 5, 2017. This work was supported in part by the Ministry of Science and Technology (Taiwan) under Grant MOST 105-2221-E-182-026 and Grant 104-2221-E-182-055 and in part by the Chang Gung Memorial Hospital, Linkou, under Grant BMRP 999. Corresponding author: C.-L. Tsai (e-mail: cltsai@mail.cgu.edu.tw).

Abstract: Visible light communications with InGaN-based light-emitting diodes (LEDs) grown on large-diameter (6-inch) and cost-effective Si (111) substrates are investigated experimentally. During epitaxial growth, the transition layers consisted of the step-graded AlGaN buffers incorporated with three low-temperature-grown (~900 °C) AlN interlayers on AlN/Si substrates that are used to compensate for thermally induced tensile stress and to maintain a reasonable crystalline quality of GaN-on-Si LEDs. Strong light absorption from Si can be prevented by fabricating a Si substrate-free InGaN LED with a composite metal coating of Al/Ag/Al multilayer, providing improved adhesive strength and reflectivity comparable to the unitary Ag film. In comparison with GaN-on-Si LEDs, stripping Si substrates combined with the use of a highly reflective bottom mirror (Al/Ag/Al multilayer) reflected a more intense emission pattern corresponding to a 2.2 times (@ 190 mA) increase in light output power in thin-film LEDs. In addition, a 1.8 times (@ 160 mA) increase in optical channel bandwidth is achieved by using thin-film LEDs as optical transmitters. A direct line-of-sight optical link using the proposed thin-film LEDs achieved data transmission rates of up to 100 Mb/s over a distance of 100 cm, indicating that the proposed LEDs have potential for use as optical transmitters in indoor visible light communications.

Index Terms: InGaN, light-emitting diodes (LEDs), Si substrate, line-of-sight optical link, visible light communications.

1. Introduction

Group III nitride semiconductors ($In_xGa_{1-x}N$ alloys) have a direct energy bandgap that is beneficial for the creation of photons through the radiative recombination process, and their emission

wavelengths can be tuned to approach the visible range simply by modifying the alloy composition. Currently, these alloys are extensively used as the active media for energy-saving visible light-emitting diodes (LEDs) [1]. Promoting the widespread use of energy-efficient LED luminaires requires replacing insulating sapphire substrates with other materials to facilitate heat dissipation during LED operation while reducing overall production costs. Among available substrates (i.e., sapphire, bulk GaN, and SiC) for the growth of nitride-based semiconductors [2]–[4], the high thermal conductivity ($\sim 150\,\mathrm{Wm^{-1}K^{-1}}$) of Si makes it a promising candidate for mass production of large-size (8-inch) GaN-on-Si LED wafers. Novel optoelectronic devices based upon such an approach, however, require a delicate stress-compensation scheme to suppress tensile thermal stress induced cracks during wafer cooling due to large lattice constant mismatch (~17%) and thermal expansion mismatch (~54%) between GaN and Si [5]–[8]. Liou *et al*. reported that the improvement in crystalline quality of InGaN-based solar cells grown on Si can be achieved by inserting a 0.1-μm-thick layer of SiCN between the n-GaN and the Si substrate [9]. As a result, solar cells fabricated using a 10-pair $In_{0.32}Ga_{0.68}N$/GaN multiple-quantum-well (MQW) as an absorption layer and grown on SiCN–Si substrates exhibit a photovoltaic efficiency as high as 5.43%. A hybrid power amplifier composed of an AlGaN/GaN high-electron-mobility transistor and a p-type metal–oxide–semiconductor field-effect transistor with a voltage gain of 17 at 3 V supply voltage can also be made from a 4-inch Si (100)/GaN/Si (111) hybrid wafer using Si-compatible bonding technology [10]. Recently, blue–violet InGaN-based laser diodes with continuous-wave lasing characteristics have been proven to be feasible even when grown on Si substrates [11].

Despite being used as solid-state lighting sources for a variety of applications such as displays, traffic signals and general lighting, etc., these visible LEDs can also be used as optical transmitters in optical wireless links for data communications [12]. Unlike radio-frequency (RF) links, LED-based visible light communications offer several advantages including low system costs, license-free operation, immunity to electromagnetic interference, network security, and high and unregulated bandwidth [12], [13]. Fahs *et al*. reported establishing an on-off-keying based optical link with a high-speed laser diode ($\lambda = 680$ nm) and a high-sensitivity integrated circuit receiver, allowing for digital signals (a $2^{31} - 1$ pseudorandom bit sequence) to be transmitted at a rate of up to 2.5 Gb/s over a 12-m distance while maintaining a bit error rate $< 10^{-3}$ [14]. In addition to high electrical-to-optical modulation bandwidth (~270 MHz) from GaN-based micro-pixelated LED (μLED) grown on Si substrates, visible light communications using these μLEDs can provide a data transmission rate of up to 400 Mbit/s [15].

This paper experimentally investigates the feasibility of visible light communications with InGaN-based LEDs grown on large-diameter (6-inch) and cost-effective Si (111) substrates using metal-organic vapor phase epitaxy (MOVPE). During epitaxial growth, the transition layers consisted of the step-graded AlGaN buffers incorporated with three low-temperature-grown (~900 °C) AlN interlayers on AlN/Si substrates, used to compensate for thermally induced tensile stress and to maintain a reasonable crystalline quality of GaN-on-Si LEDs. Although Si has good thermal and electrical properties that can help to realize a vertical-conducting InGaN LED, the downward light emitted from the active regions will be absorbed by such dissipative materials and thus cannot contribute to light output. Using wet etching along with wafer-transfer techniques, the completed Si substrate-free LEDs with a bottom reflector (hereinafter thin-film LEDs) can exhibit improved performance as compared to that of the LEDs with the Si substrate. A direct line-of-sight optical link capable of 100 Mbit/s free-space transmissions over 100 cm is accomplished using these thin-film LEDs as optical transmitters.

2. Experimental

Epiwafers of InGaN LEDs (see Fig. 1) were grown on a 6-inch Si (111) substrate using an Aixtron-2800G4 MOVPE system. Trimethylgallium (TMGa) and trimethylindium (TMIn) were used as the group-III sources, while NH_3 was used as the group-V source. Prior to growth, Si wafers were chemically treated with the H_2SO_4/H_2O_2 and buffered-oxide-etch (BOE) solutions to achieve an oxide-free, hydrogen-terminated Si surface. After in-situ high-temperature cleaning at 1050 °C in

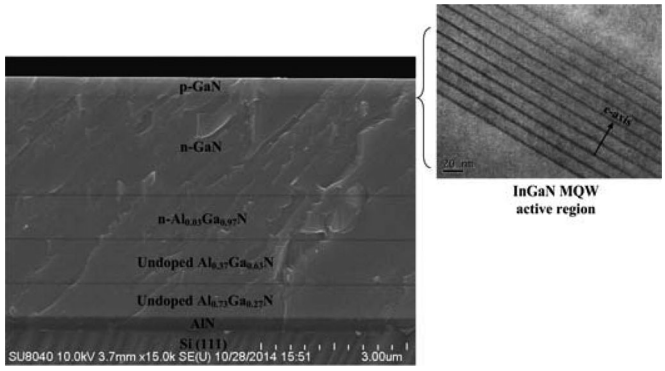

Fig. 1. SEM image of the InGaN LED grown on Si (111) substrates. Three low-temperature-grown (∼900 °C) AlN interlayers were inserted into the step-graded AlGaN buffer layers to control the stress and crystalline quality. (Inset) HRTEM image of InGaN MQWs in GaN-on-Si LEDs.

hydrogen gas, a stacked AlN epilayer was grown on Si (111) to act as a nucleation layer and to prevent the direct reaction of Si with Ga at high temperature [16]. The layered AlN epistructures were grown at temperatures of 1150, 900 and 1150 °C. Prior to the deposition of a 2-μm-thick Si-doped n-GaN ($N_d = 5 \times 10^{18}\,cm^{-3}$), a step-graded AlGaN buffer (with Al compositions of about 73%, 37% and 3%) was used as the transition layer between the AlN and GaN. To avoid severe current crowding, the last growth of $Al_{0.03}Ga_{0.97}N$ buffer was also doped with silicon ($N_d = 2 \times 10^{18}\,cm^{-3}$). In addition to being used as a decoupling layer to induce a compressive stress in the subsequent growth of (Al)GaN layers, both the growth and the thermally induced tensile stresses can also be controlled by inserting three low-temperature-grown (∼900 °C) AlN interlayers into the step-graded AlGaN buffers [5], [17]. Furthermore, the benefit of using the step-graded AlGaN buffer layers is that the relaxation of accumulated compressive strain can be alleviated as the layer thickness is sufficient to accommodate the material defects [5], [7]. The active region of GaN-on-Si LEDs was made of a 10-pair InGaN/GaN MQW for 460 nm emission. Afterward, a 25-nm-thick p-$Al_{0.2}Ga_{0.8}N$ electron blocking layer was incorporated on top of the InGaN MQW region. Deposition of the Mg-doped GaN layer terminated the growth procedure. The residual strain of the as-grown GaN-on-Si LEDs can be clarified by Raman spectroscopy. According to the Raman shift of the GaN E_2 phonon peak (567.7 cm^{-1}) with respect to that of the unstrained GaN (567.5 cm^{-1}) [18], the in-plane stress of GaN-on-Si LEDs is calculated to be 0.047 GPa. Through good control of the step-graded AlGaN buffer layers during growth, we can achieve a nearly strain-free GaN-on-Si LED.

The fabrication process of GaN-on-Si LEDs with surface-emitting geometry involves the formation of a $510 \times 510\,\mu m^2$ indium tin oxide (ITO)-coated mesa, followed by the formation of n contacts on the exposed n-GaN layer and p-contacts on part of the ITO. Finally, the LED wafer thickness was reduced to ∼300 μm using a chemical mechanical polishing machine. To fabricate the thin-film LEDs with a bottom reflector, the completed GaN-on-Si LEDs were bonded to a temporary carrier prior to the removal of the Si substrate by wet chemical etching ($HF:HNO_3 = 1:2$). Although silver (Ag) has a high reflectance in the visible wavelengths, poor adhesion to III-V semiconductors and the lack of a native passivation layer (i.e., metal oxide like Al_2O_3) limits their use as a bottom reflector for the LEDs [19]. Fig. 2 shows the measured reflectance spectra of a glass plate coated with different metallic films. The normal incidence of light impinges from the back side of the glass. Instead of epitaxial growth of the GaN epilayers on a well-polished sapphire substrate [20], the benefits of using the glass plates as a template for the metallic films coating include their high transparency in the visible wavelengths and easy availability. The root-mean-square roughness of the glass plates measured by atomic force microscopy (AFM) with a scan area of 100 μm^2 is about 0.375 nm. In the experiment, the adhesion strength of the metallic films can then be roughly tested by using a stick tape (3M Transpore Tape) as they were coated on glass with an extremely smooth surface. Although the reflection coefficients measured from the glass plates coated with a metallic

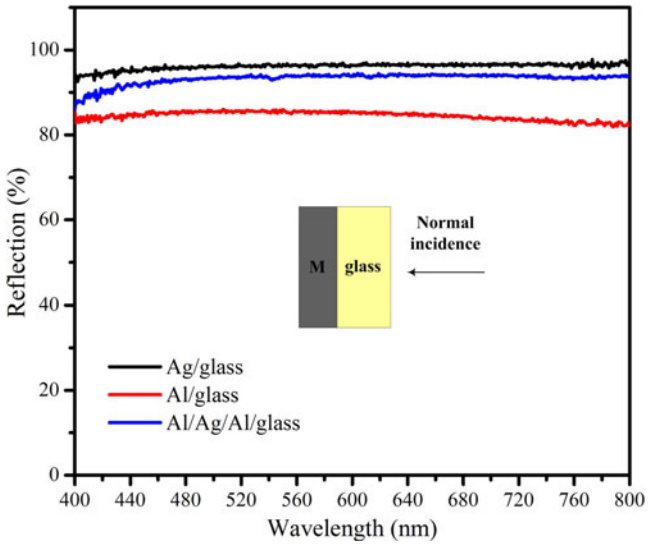

Fig. 2. Measured reflectance spectra of a glass plate coated with different metallic films. The normal incidence of light impinges from the backside of the glass.

film may deviate from those of the real structures with a metal/(Al)GaN interface, this approach still provides valuable qualitative data for the characterization of the metallic films' reflectivity given the need for good adhesion between the metal film and the underlying template. Fig. 2 shows that Al (5 nm)/Ag (150 nm)/Al (150 nm) multilayer coated on glass can provide a reflectivity comparable to that of the unitary Ag film. Compared with Al film (~150 nm), the proposed Al/Ag/Al multilayer also provides a higher reflection coefficient in the reflective spectrum over the wavelength range from 400 to 800 nm. In this multilayer structure, the first-coated Al layer functions as an adhesive layer while the last deposition of a thick Al protects the composited films against ambient moisture [21]. In addition, a 92.6% reflectivity measured at $\lambda = 460$ nm results from the highly reflective Ag layer due to the deposition of a thin (~5 nm) Al layer beneath. It should be noted that the adhesion strength between the glass and Al/Ag/Al multilayer decreases given a first-coated Al layer thickness of less than 5 nm. After dicing, the thin-film LEDs fabricated with a bottom reflector (Al/Ag/Al multilayer) were mounted onto the TO-46 headers using Ag paste, and the temporary carrier was removed by dissolving the wax adhesive. TO-packaged GaN-on-Si LEDs were also made for the purpose of comparison. Fig. 3(a) shows a schematic diagram of a completed thin-film LED. Corresponding near-field images of both InGaN LEDs at 140 mA are shown in Fig. 3(b). Because ITO films have a low sheet resistance ($R_{sh} = 20.3\,\Omega$/sq) given by the transfer length method (TLM) [22], the injected carriers (holes) from the p-contact electrode can spread uniformly over the ITO-coated mesa surface and then recombine radiatively with electrons propagated laterally along the shorter paths of the n-GaN layer with a sheet resistance of 24.5 Ω/sq. As a result, current crowding will occur near the mesa edge of the p-contact for both LEDs. In comparison with GaN-on-Si LEDs, the impact of stripping Si substrates combined with the use of a highly reflective bottom mirror produced a more intense pattern of light emission from the thin-film LEDs. Finally, the completed LEDs without epoxy encapsulation were driven by a Keithley Model 2400 source meter and the corresponding light output power was measured using a calibrated integrating optical sphere sensor (Newport Corp.).

3. Results and Discussion

Fig. 4(a) shows the XRD omega rocking curves of InGaN LEDs grown on Si substrates measured from the GaN symmetrical (0002) and GaN asymmetrical ($10\bar{1}2$) planes. The full width at

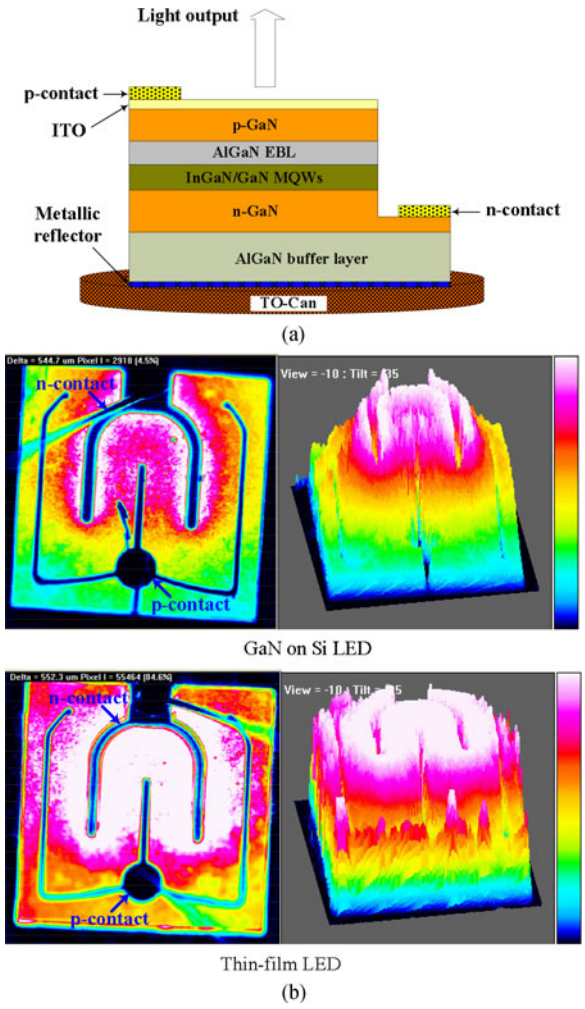

Fig. 3. (a) Schematic diagram of a completed thin-film LED. The completed device was bonded onto a TO-header without an epoxy encapsulation for characterization. (b) Near-field images of the GaN-on-Si LED and the thin-film LED at 140 mA.

half-maximum (FWHM) values of (0002) and (10$\bar{1}$2) reflections can be used to roughly estimate the amount of threading dislocations in InGaN LEDs. Using the method reported in [23], the corresponding screw and edge dislocation density of GaN-on-Si LEDs are calculated to be $\sim 1.4 \times 10^8\,\mathrm{cm}^{-2}$ and $\sim 1.2 \times 10^9\,\mathrm{cm}^{-2}$, comparable to those of previous findings [24]. In addition, the presence of several well-resolved satellite peaks in the X-ray diffraction pattern (Fig. 4(b)) together with the high contrast between the InGaN and GaN layers observed from the high-resolution transmission electron microscopy (HRTEM) image (shown in the inset of Fig. 1) are a good indicator of structural perfection and sharp interfaces of the InGaN/GaN MQW heterostructures grown on a 6-inch Si substrate. Based upon the HRXRD w-2θ scans of the GaN (0002) and GaN (10$\bar{1}$2) reflections, the MQW period and the average indium composition is estimated to be about 13.0 nm and 2.5%, respectively, for the GaN-on-Si LEDs [25]. As evaluated from temperature dependence of the photoluminescence (PL) measurements (not shown here), an anomalous optical behavior of "S-shaped" (redshift-blueshift-redshift) variations is observed in peak wavelength of our InGaN LEDs as temperature increased from 20 to 300 K. This is considered to be the result of spatial inhomogeneities of the indium distribution in InGaN MQWs caused by phase separation or spinodal decomposition [26]. Despite many material defects ($\sim 10^9\,\mathrm{cm}^{-2}$) in the as-grown InGaN LEDs, injected carriers will

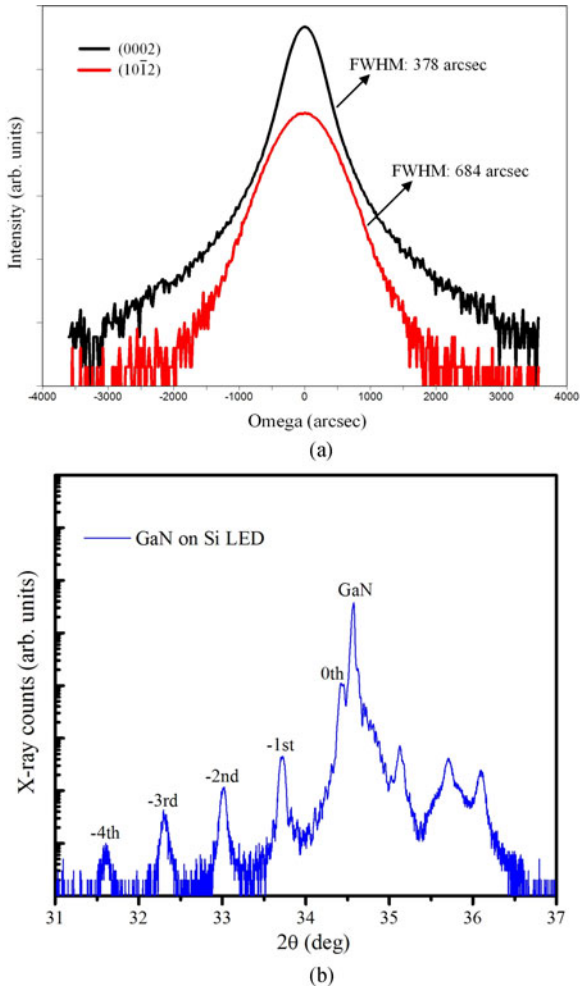

Fig. 4. (a) XRD omega rocking curves of the InGaN LEDs grown on Si substrates measured from the GaN symmetrical (0002) and GaN asymmetrical (10$\bar{1}$2) planes. (b) High-resolution X-ray diffraction (HRXRD) *w*-2θ scans of the (0002) reflections for the LEDs grown on Si substrates.

tend to recombine radiatively at these localized states instead of being captured by nonradiative recombination centers.

Fig. 5 shows the light output power and external quantum efficiency versus injection current measured at 300 K for both the GaN-on-Si LED and the thin-film LED. Due to good device-to-device uniformity of the fabricated LEDs, the respective data shown in the figure is taken from one of five test LEDs randomly selected from the same device type. Both the LEDs exhibit a forward voltage of about 2.7 V at a current of 20 mA. In addition, the equivalent series resistance extracted from the current-voltage curve (shown in the inset of Fig. 5) is estimated at 5.4 Ω for all fabricated LEDs. This indicates that the Si substrate stripping process has a negligible impact on the electrical properties of thin-film LEDs. As shown in Fig. 5, the light output power of thin-film LED increases with injection current and reaches a maximum value of 19 mW at 190 mA. The light intensity starts to degrade as operation current exceeds 205 mA. At 190 mA, a 2.2 times increase in light output power is found in the thin-film LEDs. In addition, these LEDs also have a maximum external quantum efficiency of 6.7% at 26 mA. Compared with GaN-on-Si LEDs, however, a higher droop rate in emission efficiency is found in thin-film LEDs operating at elevated current levels. Instead of being absorbed by the Si substrates, downward-emitting photons increasingly escape from the

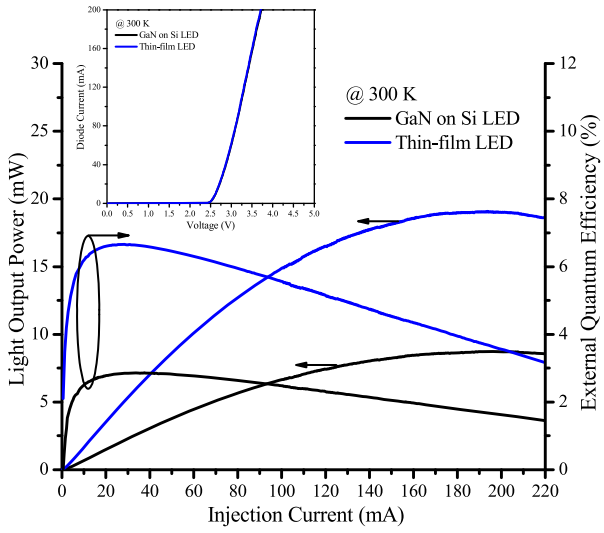

Fig. 5. Light output power and external quantum efficiency versus injection current measured at 300 K for both the GaN-on-Si LED and the thin-film LED. (Inset) Current-voltage characteristics of the fabricated InGaN LEDs.

semiconductors due to the integration of the bottom reflector, resulting in improved light output and also consistent with the result of the near-field measurements from the fabricated LEDs, as shown in Fig. 3(b). LED emission efficiency could be further improved by reducing the threading dislocation density through inserting a SiN interlayer into the underlying GaN buffers grown on Si [27] or epitaxial growth of a modified MQWs with a thin AlGaN interlayer to increase the LED's quantum efficiency [28]. In addition, the LED chips fabricated with an optimized design of the current spreading electrodes can also be mounted epitaxial-side-down to form a flip-chip packaged LED to repair the light output degraded by the current crowding [29]. For InGaN LEDs, the degradation of emission efficiency at high currents is generally known to be associated with Auger nonradiative recombination or insufficient potential barrier height of the polarization unmatched AlGaN EBL to prevent electron leakage [30]. Because both LEDs were made from the same InGaN epi-wafer, the influence of these factors on the efficiency droop is expected to be similar. At high levels of current injection, another factor to reduce the emission efficiency of InGaN LEDs is increased junction temperature resulting in more thermal carriers escaping from the MQWs and thus not contributing to light output [31]. As shown in Fig. 6, a redshift in emission wavelength was observed in both LEDs as the current injection level increases above 20 mA. As the injection current increased from 20 to 180 mA, the electroluminescence (EL) spectrum for the GaN-on-Si LED exhibits a redshift of 1.1 nm while a relatively large value of 1.8 nm was found in the thin-film LED. As mentioned before, the completed LED chips were all packaged onto the TO headers using Ag paste. Due to the poor thermal conductivity of the Ag paste ($2-25\ \mathrm{Wm^{-1}K^{-1}}$), the heat generated at the p-n junction of thin-film LEDs can not easily be conducted to the metal can package (TO-46), thus resulting in apparent light output degradation at higher current levels. However, in addition to serving as the growth substrate, Si can also be used to facilitate heat dissipation of InGaN LEDs due to its high thermal conductivity ($\sim 150\ \mathrm{Wm^{-1}K^{-1}}$) and specific heat capacity ($\sim 700\ \mathrm{Jkg^{-1}K^{-1}}$) [32]. Therefore, at elevated current levels, the influence of joule heating on this device (GaN-on-Si LED) would be rather slight despite the thermal barrier induced by the Ag paste. Further improvement in thermal properties could be achieved by using eutectic AuSi solder ($190-285\ \mathrm{Wm^{-1}K^{-1}}$) instead of the Ag paste [33] or using the metal carrier (Cu) as a heat sink [34].

To improve power efficiency as well as immunity to environmental disturbances such as multipath interference, a directed line-of-sight optical link is preferentially used for the realization of LED-based visible light communications [35]. Fig. 7 shows the experimental setup of the proposed

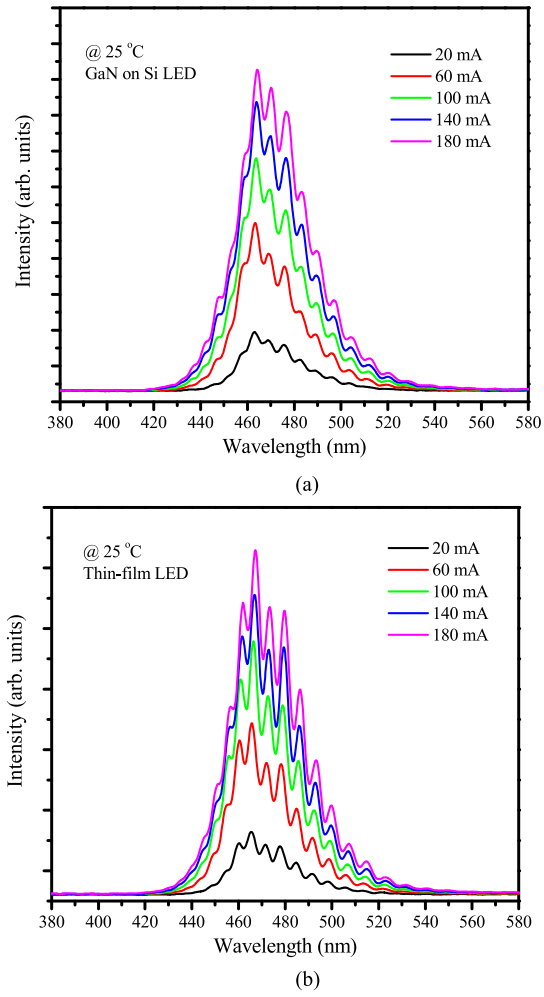

Fig. 6. EL spectrum measured at different current levels for (a) the GaN-on-Si LED and (b) the thin-film LED.

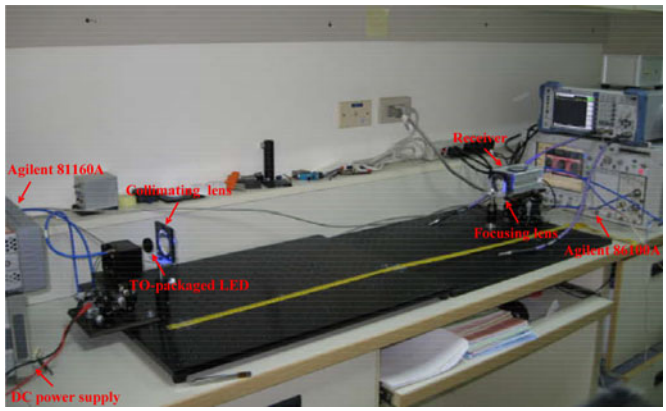

Fig. 7. Experimental setup for line-of-sight visible light communications. The distance between the light source and the receiver was set at 100 cm.

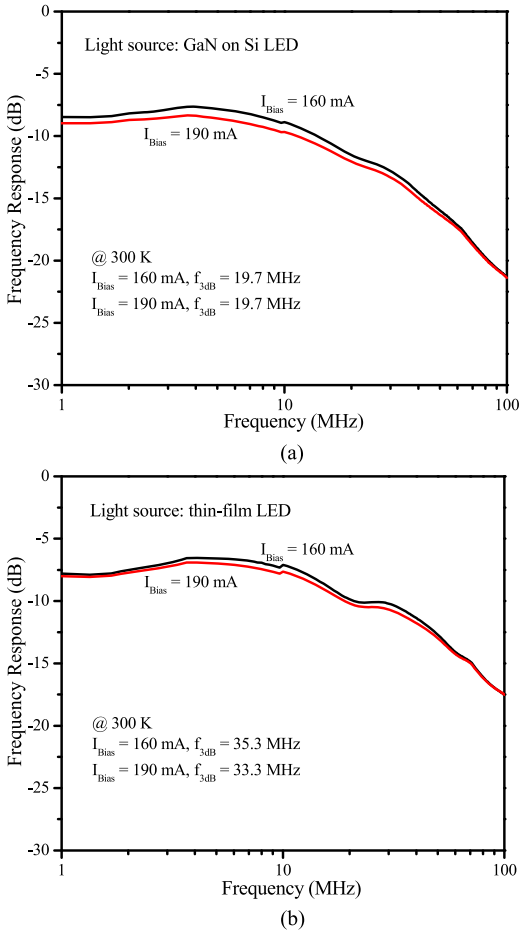

Fig. 8. Measured frequency response of an optical wireless link with the TO-packaged LEDs operating at different bias currents. The separation distance between the transmitter and the receiver is set at 100 cm.

optical communication system. Experimentally, a bias current and nonreturn-to-zero (NRZ) pseudorandom bit sequence (PRBS) generated from an Agilent 81160A pulse function arbitrary noise generator was combined in a bias tee and fed to the TO-packaged LEDs. The collimated light propagation through a given distance (100 cm) in free space is collected by the optical receiver (Pacific AD500-9-400M-TO5) using a light coupling lens (Edmund Optics, 40.0 mm Dia. x 60.0 mm FL uncoated plano-convex lens) and then analyzed by a wide-bandwidth sampling oscilloscope (Agilent 86100A). Taking propagation loss into account, the fabricated thin-film LEDs is preferred in such optical systems due to its enhanced light output as compared to that of GaN-on-Si LEDs.

A similar experimental setup, including the bias tee-driven transmitter, light coupling lens (two plano-convex lenses), optical receiver (Pacific AD500-9-400M-TO5), and the Rohde & Schwarz ZVL network analyzer, was used to investigate the system bandwidth of LED-based visible light communications. Fig. 8 shows the measured frequency response of an optical wireless link with the TO-packaged LEDs operating at different bias currents. The separation distance between the transmitter and the receiver is set at 100 cm. At a bias current (I_{Bias}) of 160 mA, the 3-dB modulation bandwidth (f_{3dB}) of 35.3 MHz achieved as the thin-film LED was used as an optical transmitter, which is higher than that obtained using the GaN-on-Si LED ($\sim$19.7 MHz). In addition, the presence of Joule heating may be responsible for the observation of the limited system bandwidth as both LEDs were operated at elevated current levels. At the receiving terminal, the

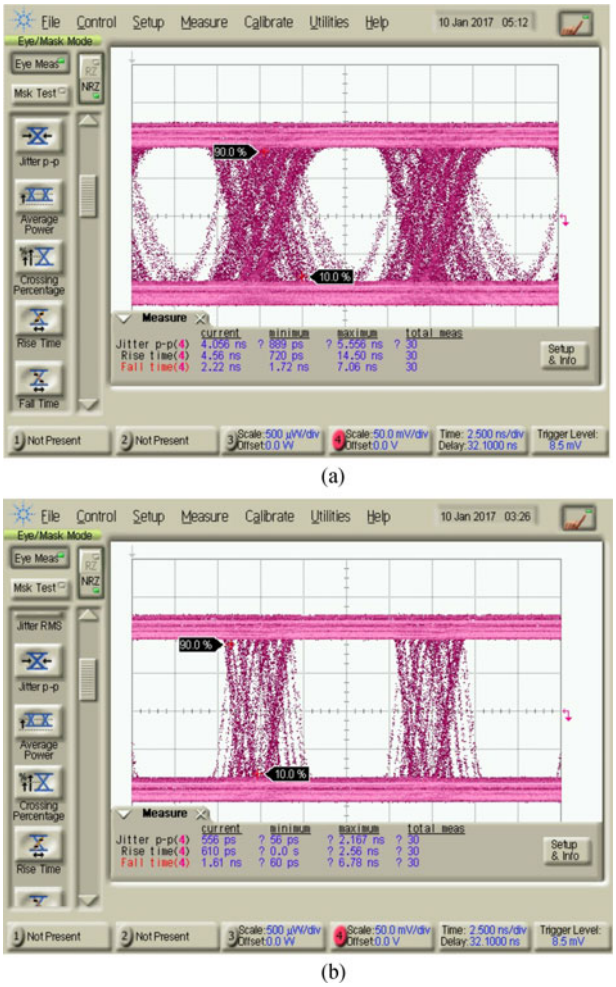

Fig. 9. Eye diagrams measured at 100 Mbit/s with $V_{PP} = 5$ V and PRBS $= 2^7 - 1$ for (a) the GaN-on-Si LEDs and (b) the thin-film LEDs operating at $I_{Bias} = 160$ mA. The distance between the transmitter and the receiver is set at 100 cm.

light intensity is about 5.04 mW at $I_{Bias} = 160$ mA, as measured by using an optical power meter (Anritsu ML910B) with an optical power sensor (Anritsu MA9411A) located at exactly focusing point of the plano-convex lens, as the thin-film LED was used as an optical transmitter. Therefore, the light coupling efficiency of such a transmission system is roughly estimated as 36.3% provided the original light intensity of the LEDs was obtained from the same optical power meter. The carrier lifetime (τ_c) of the LEDs is known to be correlated with the lifetime of injected carriers ruined through the radiative or nonradiative recombination process and can be described as [36]

$$\frac{1}{\tau_c} = \frac{1}{\tau_r} + \frac{1}{\tau_{nr}}$$

where $\tau_{r(nr)}$ denotes the radiative (nonradiative) recombination lifetime. As extracted from the slope of the semi-logarithmic I-V curve, the ideality factor is, respectively, estimated as 2.09 and 2.02 for the GaN-on-Si LED and the thin-film LED. The higher ideality factor (i.e., > 2) in the GaN-based LEDs could be attributed to the defect-assisted tunneling current caused by the structural defects, Mg-H complexes, and impurity-induced vacancies [37]. However, the similar value of the ideality factor in both LEDs provides clear evidence of the nearly identical influence of the material defect-related nonradiative recombination on carrier lifetime or device performance. In the experiment, all

fabricated LEDs not only have the same InGaN/GaN MQW epistructures, but also have identical light-emitting geometries and current injection schemes, as shown in Fig. 3. Therefore, both LEDs should have a similar lifetime-limited bandwidth because an equal number of carriers (or the current density) will be injected into the MQW active regions to participate in the recombination process as these LEDs were biased at the same currents [38]. However, after light propagation through a given distance (100 cm) in free space, an increase in the optical signal level detected at the receiver can help increase system bandwidth provided a high-power LED (e.g., thin-film LED in this study) was used as the optical transmitter [39]. Fig. 9(a) and (b), respectively, show the eye diagram measured from the GaN-on-Si LED and the thin-film LED operating at $I_{Bias} = 160$ mA. Both LED were operated at 100 Mbit/s with a pattern length of $2^7 - 1$ and a peak-to-peak voltage (V_{pp}) of 5 V. A clear and good open eye diagram at a data transmission rate of 100 Mbit/s is observed for the thin-film LEDs, while the quality of the eye diagram degrades as the GaN-on-Si LEDs were used as optical transmitters. This is due to a larger optical power from the thin-film LEDs improving the received signal-to-noise ratio of the optical transmission system [39]. As shown in Fig. 9(b), a directed line-of-sight optical link capable of 100 Mbit/s data transmission over a 100 cm distance in free space is feasible with the proposed thin-film LEDs used as optical transmitters. The performance of LED-based visible light communications could be further improved by using pre-emphasis and AC-coupled modulation technology to achieve high-speed data transmissions [40].

4. Conclusion

We demonstrate the fabrication and characterization of InGaN LEDs grown on a Si substrate using MOVPE. With the use of a step-graded AlGaN buffer layer incorporated with three low-temperature-grown ($\sim$900 °C) AlN interlayers to control thermally induced tensile stress, a 5.5-μm-thick crack-free InGaN LED epilayer with reasonable crystalline quality was successfully realized on a 6-inch Si substrate. In these LEDs, HRTEM and XRD analyses also revealed structural perfection in their periodic $In_{0.14}Ga_{0.86}N$/GaN MQW active regions emitting at $\lambda = 460$ nm. Despite defect formation during LED growth, the occurrence of indium compositional fluctuation in InGaN (confirmed from the temperature dependent PL measurements) facilitates radiative carrier recombination at these localized states. A composite metal coating of Al/Ag/Al multilayer acts as the bottom reflector of the Si substrate-free LEDs, providing improved adhesive strength and comparable reflectivity with respect to the unitary Ag film. In comparison with GaN-on-Si LEDs, the thin-film LEDs provide a more intense pattern of light emission corresponding to a 2.2 times (at 190 mA) increase in light output power. Owing to an increase in received optical power at the receiver, the 3-dB modulation bandwidth of an optical wireless link with the thin-film LEDs is 15.6 MHz higher (i.e., 35.3 versus 19.7 MHz) than that obtained using the GaN-on-Si LEDs. In free-space optical communication experiments with a direct optical link between the transmitter and the receiver, data was successfully transmitted at a rate of 100 Mbit/s over a distance of 100 cm using the proposed thin-film LEDs.

References

[1] S. Pimputkar, J. S. Speck, S. P. DenBaars, and S. Nakamura, "Prospects for LED lighting," *Nature Photon.*, vol. 3, no. 4, pp. 180–182, Apr. 2009.
[2] F. K. Yam and Z. Hassan, "InGaN: An overview of the growth kinetics, physical properties and emission mechanisms," *Superlattices Microstruct.*, vol. 43, pp. 1–23, 2008.
[3] H. Masui, S. Nakamura, S. P. DenBaars, and U. K. Mishra, "Nonpolar and semipolar III-nitride light-emitting diodes: Achievements and challenges," *IEEE Trans. Electron Devices*, vol. 57, no. 1, pp. 88–100, Jan. 2010.
[4] T. Akasaka, H. Gotoh, H. Nakano, and T. Makimoto, "Blue-purplish InGaN quantum wells with shallow depth of exciton localization," *Appl. Phys. Lett.*, vol. 86, 2005, Art. no. 191902.
[5] S. Raghavan and J. Redwing, "Growth stresses and cracking in GaN films on (111) Si grown by metalorganic chemical vapor deposition. II. Graded AlGaN buffer layers," *J. Appl. Phys.*, vol. 98, 2005, Art. no. 023515.
[6] A. Dadgar, C. Hums, A. Diez, F. Schulze, J. Bläsing, and A. Krost, "Epitaxy of GaN LEDs on large substrates: Si or sapphire?" *Proc. SPIE*, vol. 6355, 2006, Art. no. 63550R.
[7] D. Zhu *et al.*, "InGaN/GaN LEDs grown on Si(111): Dependence of device performance on threading dislocation density and emission wavelength," *Phys. Status Solidi C*, vol. 7, no. 7/8, pp. 2168–2170, 2010.

[8] Z. Y. Li *et al.*, "High-efficiency and crack-free InGaN-based LEDs on a 6-inch Si (111) substrate with a composite buffer layer structure and quaternary superlattices electron-blocking layers," *IEEE J. Quantum Electron.*, vol. 50, no. 5, pp. 354–363, May 2014.
[9] B. W. Liou, "InxGa1-xN–GaN–based solar cells with a multiple-quantum-well structure on SiCN–Si(111) substrate," *IEEE Photon. Technol. Lett.*, vol. 22, no. 4, pp. 215–217, Feb. 2010.
[10] H. S. Lee, K. Ryu, M. Sun, and T. Palacios, "Wafer-level heterogeneous integration of GaN HEMTs and Si (100) MOSFETs," *IEEE Electron Device Lett.*, vol. 33, no. 2, pp. 200–202, Feb. 2012.
[11] Y. Sun *et al.*, "Room-temperature continuous-wave electrically injected InGaN-based laser directly grown on Si," *Nature Photon.*, vol. 10, pp. 595–599, Sep. 2016.
[12] L. Grobe *et al.*, "High-speed visible light communication systems," *IEEE Commun. Mag.*, vol. 51, no. 12, pp. 60–66, Dec. 2013.
[13] S. Rajagopal, R. D. Roberts, and S. K. Lim, "IEEE 802.15.7 visible light communication: Modulation schemes and dimming support," *IEEE Commun. Mag.*, vol. 50, no. 3, pp. 72–82, Mar. 2012.
[14] B. Fahs, A. J. Chowdhury, and M. M. Hella, "A 12-m 2.5-Gb/s lighting compatible integrated receiver for OOK visible light communication links," *J. Lightw. Technol.*, vol. 34, no. 16, pp. 3768–3775, Aug. 2016.
[15] P. Tian *et al.*, "Characteristics and applications of micro-pixelated GaN-based light emitting diodes on Si substrates," *J. Appl. Phys.*, vol. 115, 2014, Art. no. 033112.
[16] K. L. Lin *et al.*, "Growth of GaN film on 150 mm Si (111) using multilayer AlN/AlGaN buffer by metal-organic vapor phase epitaxy method," *Appl. Phys. Lett.*, vol. 91, 2007, Art. no. 222111.
[17] A. Reiher, J. Bläsing, A. Dadgar, A. Diez, and A. Krost, "Efficient stress relief in GaN heteroepitaxy on Si(111) using low-temperature AlN interlayers," *J. Crystal Growth*, vol. 248, pp. 563–567, 2003.
[18] J. Park, K. M. Song, S. H. Moon, and S. W. Ryuz, "Reduced indium fluctuation in InGaN quantum well grown on GaN air bridge," *J. Electrochem. Soc.*, vol. 157, no. 7, pp. H739–H741, 2010.
[19] M. Khizar and Y. M. A. Raja, "AlGaN-based deep ultraviolet light emitting diodes with reflection layer," *Proc. SPIE*, vol. 6473, 2007, Art. no. 64730V.
[20] C. C. Lin and C. T. Lee, "GaN-based resonant-cavity light-emitting diodes with top and bottom dielectric distributed Bragg reflectors," *IEEE Photon. Technol. Lett.*, vol. 22, no. 17, pp. 1291–1293, Sep. 2010.
[21] M. Gruber, T. Seiler, and A. C. Wei, "High-reflectance composite metal coatings for planar-integrated free-space optics," *Appl. Opt.*, vol. 45, no. 4, pp. 662–667, Feb. 2006.
[22] R. Jackson and S. Graham, "Specific contact resistance at metal/carbon nanotube interface," *Appl. Phys. Lett.*, vol. 94, 2009, Art. no. 012109.
[23] S. Krishna *et al.*, "Correlation of growth temperature with stress, defect states and electronic structure in an epitaxial GaN film grown on c-sapphire via plasma MBE," *Phys. Chem. Chem. Phys.*, vol. 18, pp. 8005–8014, 2016.
[24] D. Zhu *et al.*, "Efficiency measurement of GaN-based quantum well and light-emitting diode structures grown on silicon substrates," *J. Appl. Phys.*, vol. 109, 2011, Art. no. 014502.
[25] S. Q. Zhou *et al.*, "An approach to determine the chemical composition in InGaN/GaN multiple quantum wells," *J. Crystal Growth*, vol. 263, pp. 35–39, 2004.
[26] Y. H. Cho *et al.*, "S-shaped" temperature-dependent emission shift and carrier dynamics in InGaN/GaN multiple quantum wells," *Appl. Phys. Lett.*, vol. 73, no. 10, pp. 1370–1372, 1998.
[27] S. Kimura *et al.*, "Optical properties of InGaN/GaN MQW LEDs grown on Si (111) substrates with low threading dislocation densities," *Proc. SPIE*, vol. 8986, 2014, Art. no. 89861H.
[28] S. Kimura, H. Yoshida, T. Ito, A. Okada, K. Uesugi, and S. Nunoue, "High-efficiency blue LEDs with thin AlGaN interlayers in InGaN/GaN MQWs grown on Si (111) substrates," *Proc. SPIE*, vol. 9748, 2016, Art. no. 97481U.
[29] W. C. Chong and K. M. Lau, "Performance enhancements of flip-chip light-emitting diodes with high-density n-type point-contacts," *IEEE Electron Device Lett.*, vol. 35, no. 10, pp. 1049–1051, Oct. 2014.
[30] J. Piprek, "Efficiency droop in nitride-based light-emitting diodes," *Phys. Status Solidi A*, vol. 207, no. 10, pp. 2217–2225, 2010.
[31] C. Huh, W. J. Schaff, L. F. Eastman, and S. J. Park, "Temperature dependence of performance of InGaN/GaN MQW LEDs with different indium compositions," *IEEE Electron Devices Lett.*, vol. 25, no. 2, pp. 61–63, Feb. 2004.
[32] S. M. Sze, *Physics of Semiconductor Devices*, 2nd ed. New York, NY, USA: Wiley, 1981, App. H.
[33] D. D. Evans and Z. Bok, "AuSi and AuSn eutectic die attach case studies from small (12 mil) to large (453 mil) die," in *Proc. Int. Symp. Microelectron.*, Carlsbad, CA, USA, 2010, pp. 898–905.
[34] T. Egawa and B. A. B. A. Shuhaimi, "High performance InGaN LEDs on Si (111) substrates grown by MOCVD," *J. Phys. D, Appl. Phys.*, vol. 43, 2010, Art. no. 354008.
[35] C. L. Tsai and C. T. Yen, "SU-8 planarized InGaN light-emitting diodes with multipixel emission geometry for visible light communications," *IEEE Photon. J.*, vol. 7, no. 1, Feb. 2015, Art. no. 1600109.
[36] M. Fukuda, *Optical Semiconductor Device*. New York, NY, USA: Wiley, 1999.
[37] X. A. Cao, E. B. Stokes, P. M. Sandvik, S. F. LeBoeuf, J. Kretchmer, and D. Walker, "Diffusion and tunneling currents in GaN/InGaN multiple quantum well light-emitting diodes," *IEEE Electron Device Lett.*, vol. 23, no. 9, pp. 535–537, Sep. 2002.
[38] J. J. D. McKendry *et al.*, "Visible-light communications using a CMOS-controlled micro-light-emitting-diode array," *J. Lightw. Technol.*, vol. 30, no. 1, pp. 61–67, Jan. 2012.
[39] P. Deng, M. Kavehrad, and M. A. Kashani, "Nonlinear modulation characteristics of white LEDs in visible light communications," in *Proc. Opt. Fiber Commun. Conf.*, 2015, Paper W2A.64.
[40] H. Li, X. Chen, J. Guo, Z. Gao, and H. Chen, "An analog modulator for 460 MB/S visible light data transmission based on OOK-NRS modulation," *IEEE Wireless Commun.*, vol. 22, no. 2, pp. 68–73, Apr. 2015.